72395

Micropoikilitic Impact Melt Breccia
St. 2, 536.4 g

INTRODUCTION

72395 is a fine-grained, clast-bearing impact melt with a poikilitic texture. It was sampled as typical groundmass of Boulder 2, Station 2 (see section on Boulder 2, Station 2, Fig. 1). Although no definitive geochronological data exist, a general assumption is that 72395 crystallized at the same time as other melts of similar petrography and chemistry at the Apollo 17 site, i.e. 3.86 Ga ago. The sample, 12 x 9 x 5.5 cm, is angular, tabular, and light olive gray (N5Y 6/1). It is tough and homogeneous. Its exposed surface (T,N,W) has many zap pits and is knobby and rounded. The broken surface (S, E,B) is angular and hackly (Fig. 1). Vugs are present on the broken surface, ranging from 0.2 to 2 mm. They tend to be irregular but some are elongate, and many are lined with drusy crystal terminations.

72395 is typical of the samples from Boulder 2, and has only a few clasts larger than a few millimeters. Plagioclases and pale green olivine are the most abundant. The few large lithic clasts are typically fine-grained feldspathic rocks, including granulites. The groundmass contains abundant vesicles smaller than 25 microns, and consists mainly of plagioclase and pigeonite. The pigeonite forms small oikocrysts (less than 100 microns). The smaller clasts are difficult to distinguish from groundmass phases. The total clast content of the less-than- 1-mm. fraction is probably 10 to 20%.

Most of the studies of 72395 were conducted under a consortium led by the Caltech group (Dymek *et al.*, 1977). Following chipping of a few small pieces for petrographic study, a slab was cut across 72395 (Fig. 2). Many other small pieces and two larger end pieces were obtained (Fig. 3).

Figure 1: Broken surface of 72395. The sample is homogeneous and structureless, and few clasts are visible at this scale. Slit vesicles are common. The dark feature in the center is a vuggy area lined with pyroxene and plagioclase crystals. Scale in centimeters S-73-16052.

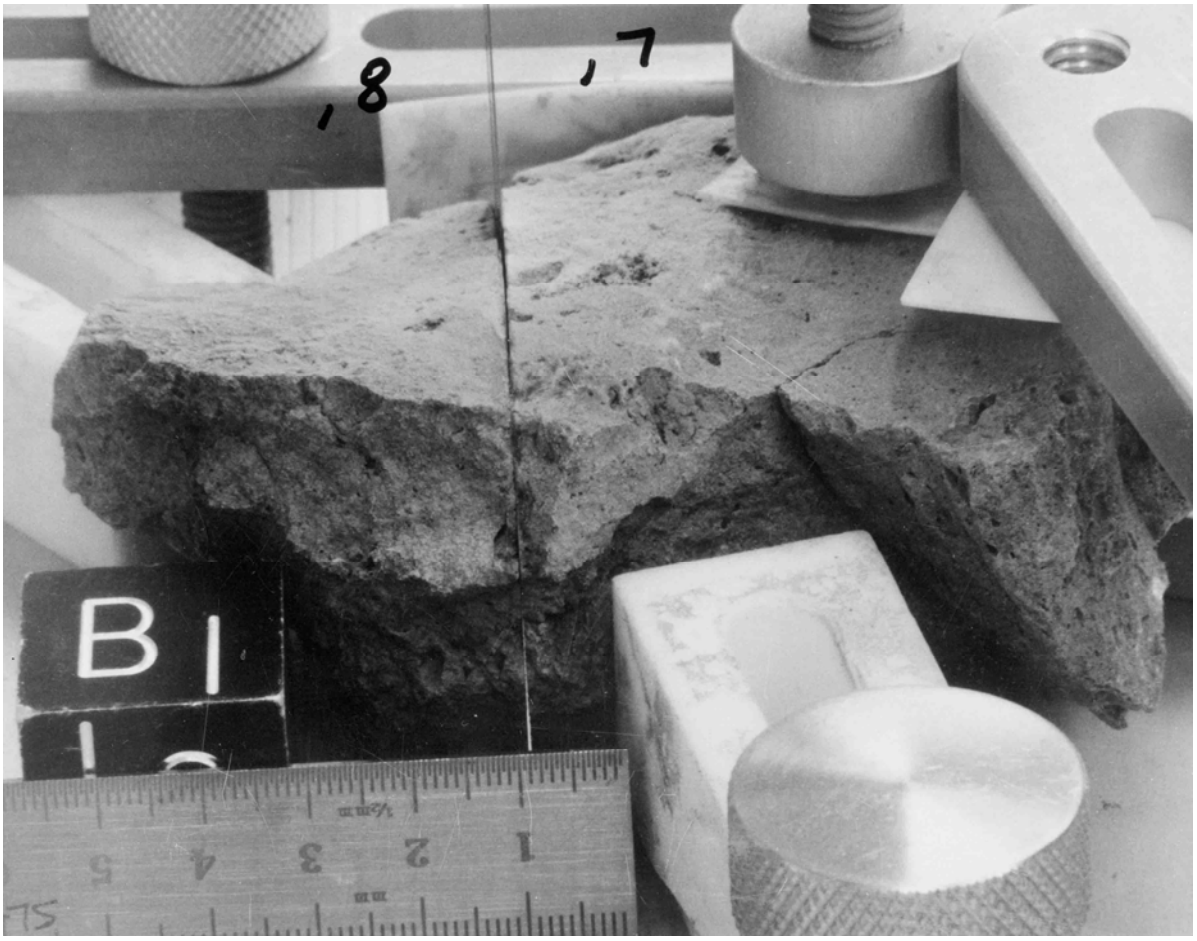

Figure 2: First cut across 72395. The second cut to produce a stab was made in, 8. Cube is 2.54 cm across. S-76-21619.

PETROGRAPHY

All five samples from Boulder 2 are very similar in petrography. Dymek *et* al. (1977) gave detailed descriptions of the petrography subsequent to the brief description by Albee *et al.* (1974b). They did not give separate descriptions of the petrography, and that practice is for the most part followed here. 72395 has the most thin sections and will be the "type" for description. The mineral diagrams for all 5 samples will be included in this section for ease of comparison.

The samples are rather homogeneous and consist of several percent clasts (I mm to 1 cm) in a fine-grained crystalline matrix. The matrix (grains less than 1 mm) is composed of abundant tiny clasts and a groundmass that crystallized from the melt (Fig. 4a) (Dymek et al., 1976a, Simonds *et al.,* 1974). Simonds *et al.,* (1974) referred to these samples as "matrix supported breccias" to emphasize the abundance of fine-grained material. They labeled 72395 as clast-rich ophitic, with matrix feldspars 10 to 40 mignons long and matrix mafic minerals 20 to 100 microns across. The texture appears to be distinct from other coarser poikilitic boulders at the Apollo 17 landing site. Dymek *et al.* (1977) drew a distinction between clasts and groundmass at 100 microns grain size. Nonetheless, the distinction of clastic material and melt-crystallized material in the <100 micron fraction is not definite. The total amount of clastic material appears to be about 10 to 20%. Voids, approximately 10% of each sample, are commonly 1 to 25 micron dispersed angular pores, with some slit vesicles up to 250 microns long. Other vugs and vesicular pods are present. In 72395 a few areas consist of pyroxene "shells" enclosing glass of granitic composition; Dymek *et al.* (1977) believe that these represent a residual liquid from the crystallization of the melt, rather than relict clasts.

The groundmass of all samples consists of an interlocking network of tiny pyroxene oikocrysts that enclose abundant chadacrysts of plagioclase. Olivine occurs as

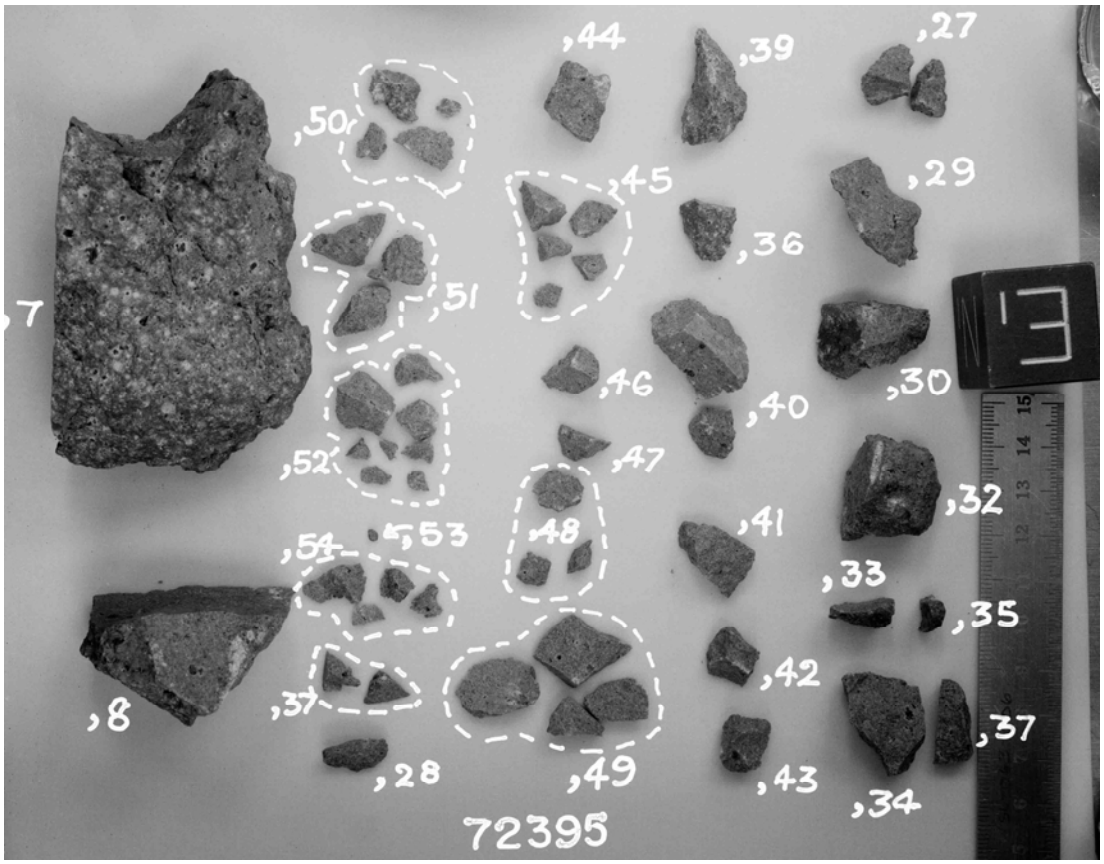

Figure 3: End pieces, 7 and, 8 and numerous smaller pieces of 72395. The slab pieces, 9 and, 10 and other small pieces are not shown. End piece, 7 shows the exterior surface with zap pits. Cube is 2 cm. S-74-15103.

angular, irregularly-shaped grains between the pyroxene oikocrysts and between pyroxene and plagioclase. Ilmenite forms irregularly-shaped grains, up to a few hundred microns long, with a sieve-texture (enclosing pyroxene and plagioclase). Engelhardt (1979) noted that ilmenite started crystallization after pyroxene started and finished crystallization after pyroxene finished. Ilmenite contains chromite and rutile lamellae and there is some baddelyite at ilmenite margins. There is some K-rich mesostasis. Troilite and lesser Fe-metal are present. According to Dymek et al. (1977), the paragenetic sequence was plagioclase followed by olivine, then low-Ca pyroxene, then high-Ca pyroxene. Olivine ceased at about the same time as high-Ca pyroxene entry, and a reaction relationship of olivine with the melt to produce the low-Ca pyroxene is suggested by resorbed-appearing olivine cores to oikocrysts. Ilmenite and other minor phases completed the crystallization.

Dymek et al. (1977) listed the phase abundances, phase compositions, and the bulk-chemical composition (from a microprobe point count) of 72395 (Table 1). The tabulated phase compositions appear to represent those in the melt groundmass, not clasts. Dymek et al. (1977) also diagrammed the mineral compositions for the five individual samples, reproduced here as Fig. 5 (plagioclases), Fig. 6 (pyroxenes), and Fig. 7 (olivines and Fe-Ti oxides), which show the general similarity of the samples. These diagrams do not distinguish clasts from groundmass phases, but they are distinguished on a summary diagram for all rocks, reproduced here as Fig. 8. The majority of the oikocrysts are pigeonite ($En_{75}Wo_2$ to $En_{65}Wo_{10}$), with some high-Ca types ($En_{54}Wo_{28}$ to $En_{45}Wo_{40}$). The chadacrysts have a small range in composition (An_{92} to An_{85}), but laths and blocky plagioclases between the oikocrysts have a wider range (An_{95} to An_{79}). The olivine in the groundmass has a narrow compositional range from Fo_{72} to Fo_{68}.

Most of the clasts in all the samples are single mineral crystals.

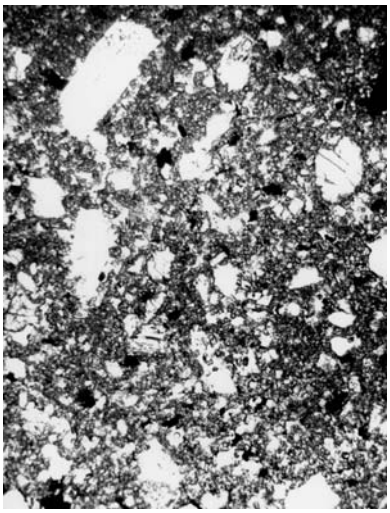

a

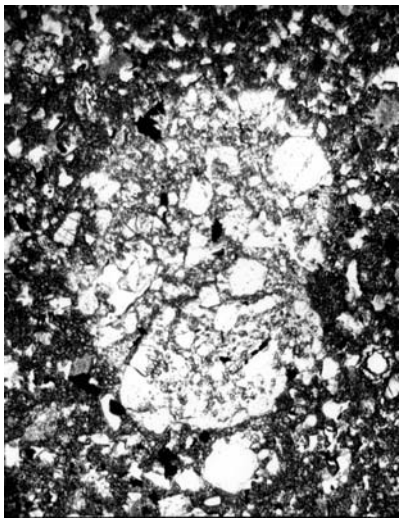

b

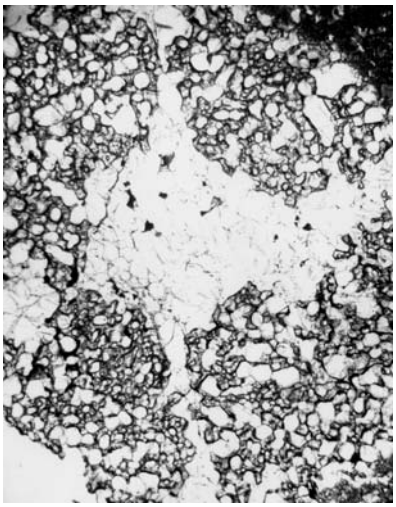

c

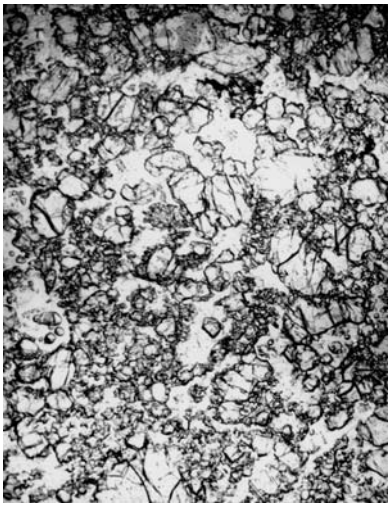

d

e

Figure 4: Photomicrographs of 72395,77. All plane transmitted light, all about 1 m field of view.
a) Melt groundmass and small clasts (larger white areas), mainly plagioclases with lesser mafic minerals.
b) feldspathic granulite clast, evidently a metamorphosed breccia.
c) coarser poikilitic feldspathic granulite clast, of less obvious precursor material. Chadacrysts (white) are plagioclases, oikocrysts (darker) are dominantly low-Ca pyroxene.
d) mafic granulite
e) devitrified plagioclase (grayer areas) and ilmenite (black) in a coarse anorthositic fragment.

Plagioclase is the most abundant, then olivine; low- and high-Ca pyroxene, ilmenite, Fe-Co-Ni metal, and pink spinel clasts are present (Dymek et al., 1976a). They are typically rounded to subangular, and a few show shock effects. Some display rims that are either overgrowths of the same phase or different minerals (coronas).The most prominent coronas are on pink spinets. Clast mineral compositions are included in Figures 5 to 7 for individual rocks, and distinguished on the summary diagram of Fig. 8. The clasts show a much wider range of compositions than do the groundmass minerals. Plagioclase clasts are generally unzoned, but many show conspicuous reaction rims. The most prominent reaction rims are on grains more sodic than the groundmass plagioclases, and many of these sodic rimmed grains have clouded cores. The olivines include many examples zoned to their rims by reaction with the melt, and some are mantled by low-Ca pyroxene. Both high- and low-Ca pyroxenes have overgrowth rims, and typically there is little difference in composition between clast rim and core, but some cores are distinctly more magnesian (Fig. 8); rims tend to have compositions similar to groundmass pyroxenes. Ilmenite and metal clasts typically occur with rounded to amoeboid forms. The ilmenite clasts contain tiny globules of metal, troilite, plagioclase, and pyroxene, unlike any seen in any lithic clast in Boulder 2.

Most of the lithic clasts are of feldspathic highlands lithologies, but there is a range of textures, grain sizes, and compositions. The most abundant group, termed anorthosites by Dymek et al. (1977), are typically fine-grained, and most are recrystallized feldspathic granulites (Figs. 4 b,c). They grade with increasing mafic content into anorthositic troctolites and norites (Fig. 4d). A few cases are poikilitic, with oikocrysts up to 3 mm. One type of anorthositic fragment was distinguished by

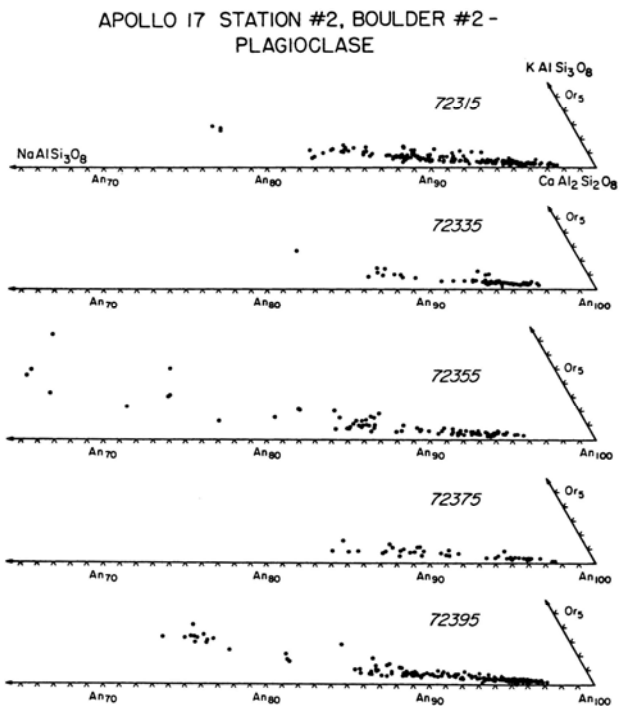

Figure 5: Compositions of plagioclases in 72315, 72335, 72355, 72375, and 72395 (Dymek et al., 1976a).

Dymek et al. (1977) for its ilmenite content of up to 10% and its brown coloring; its plagioclases are shocked and partly devitrified (Fig. 4e). A few clasts of gabbro, troctolite, and dunite are present, including one troctolite similar to 76535, though more granulated and recrystallized. The dunites (Fo_{70-77}) are more iron-rich than the dunite 72415.

CHEMISTRY

Chemical analyses of bulk rock (groundmass plus clasts) are given in Table 2; the major element analyses agree well with that derived by Dymek a al. (1976a) (Table 1). The rare earth elements are plotted as Figure 9, with other Boulder 2, Station 2 data for comparison. These chemical data were originally reported with little discussion. The samples have a low-K Fra Mauro basalt composition, similar to many other impact melt samples at the Apollo 17 site. All the Boulder 2 samples are similar, the incompatible element abundances for 72395 are higher than the average. The samples clearly have meteoritic contamination. Laul and Schmitt (1974a) identified the siderophiles with Group 3, attributed to Serenitatis, and again like many other impact melts of low-K Fra Mauro composition at the Apollo 17 site. Jovanovic and Reed (1974a, 1975, 1980), who made analyses of leaches and residues from leaching, identified the Cl (residual)/P2O5 ratio with an Apollo 11,12, and 15 basalt line, but the significance of such an identification is not apparent.

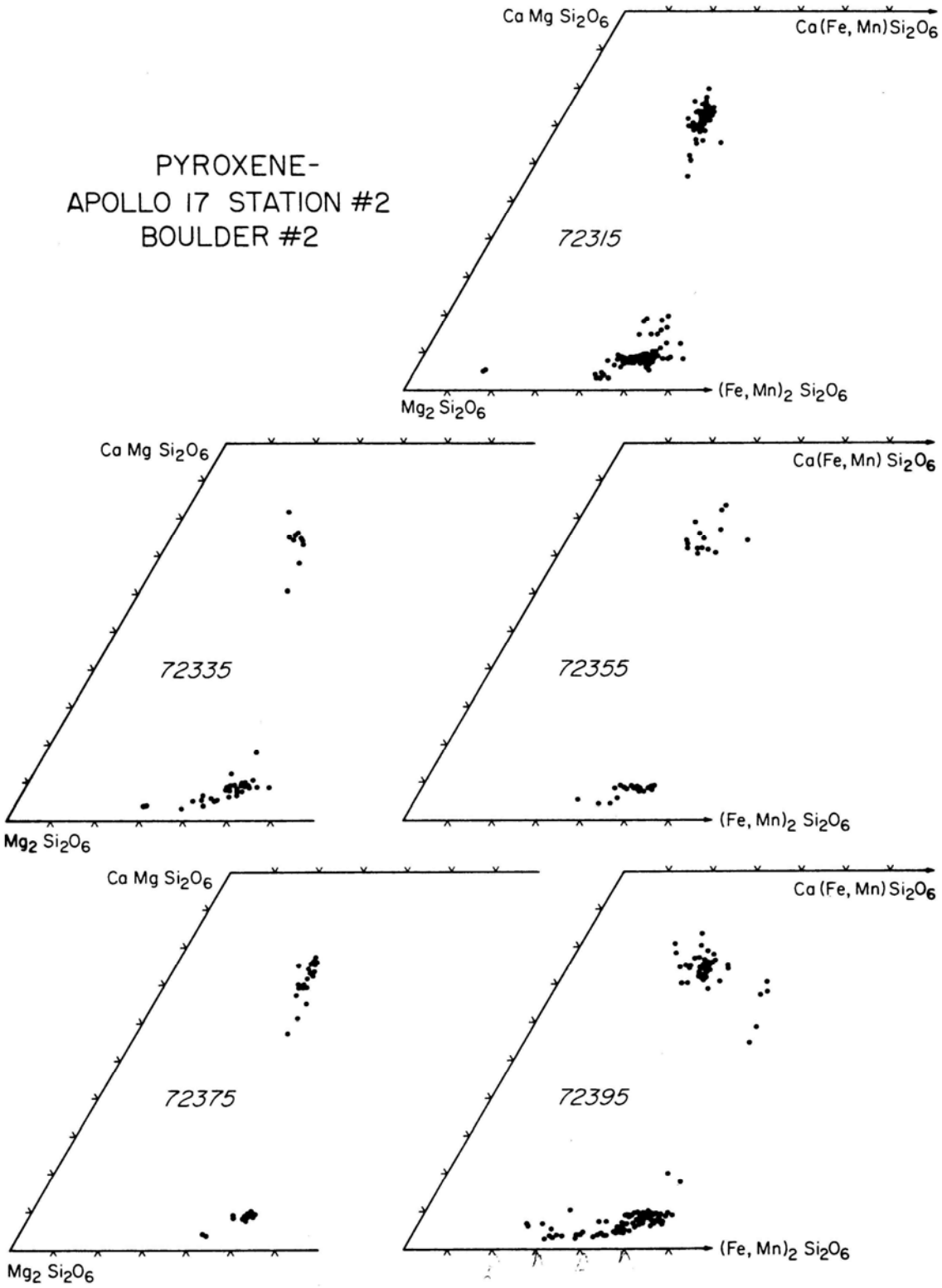

Figure 6: Compositions of pyroxenes in 72315, 72335, 72355, 72375, and 72395 (Dymek et al., 1976a).

Table 1: Phase abundances, "average" phases compositions, and bulk chemical composition derived from point-counting of 72395 (Dymek et al., 1976a).

	Plag.	Low-Ca pyx	High-Ca pyx	Olivine	Ilmenite	Troilite*	Metal*	Ca-Phos.†	Mesostasis	Bulk-composition
Vol.%	56.2_1	25.4_0	5.9_8	8.8_5	1.3_4	0.1_5	0.0_8	0.9_6	1.0_3	Calculated
$\pm 1\sigma$	2.0_8	1.4_1	0.6_8	0.8_2	0.3_2	0.1_0	0.0_8	0.2_7	0.2_8	(1307
Wt.%	50.4_3	28.4_4	6.5_6	10.2_3	2.0_0	0.2_3	0.2_1	1.0_1	0.8_9	points)
P_2O_5	n.a.	n.a.	n.a.	n.a.	n.a.	n.a.	n.a.	43.15	0.08	0.44
SiO_2	46.67	53.53	50.81	37.66	0.21	n.a.	n.a.	—	57.98	46.47
TiO_2	0.02	0.90	1.87	0.09	54.16	0.01	<0.01	—	1.82	1.50
Al_2O_3	33.51	0.99	1.95	0.02	<0.01	n.a.	n.a.	—	23.14	17.52
Cr_2O_3	n.a.	0.50	0.64	0.15	0.44	n.a.	n.a.	—	0.03	0.20
CaO	17.78	2.43	18.74	0.16	n.a.	0.08	0.01	54.54	5.29	11.50
MgO	0.09	26.36	17.08	35.76	6.56	0.03	<0.01	—	0.76	12.46
FeO	0.25	15.42	8.65	26.24	37.38	63.17	92.58	—	1.40	8.96
MnO	n.a.	0.19	0.21	0.32	0.46	n.a.	n.a.	—	<0.01	0.11
BaO	<0.01	n.a.	n.a.	n.a.	n.a.	n.a.	n.a.	—	0.90	0.01
Na_2O	1.51	0.06	0.17	n.a.	n.a.	n.a.	n.a.	—	0.53	0.79
K_2O	0.13	n.a.	n.a.	n.a.	n.a.	n.a.	n.a.	—	7.21	0.13
ZrO_2	n.a.	n.a.	n.a.	n.a.	0.01	n.a.	n.a.	—	0.07	<0.01
V_2O_3	n.a.	n.a.	n.a.	n.a.	<0.01	n.a.	n.a.	—	n.a.	<0.01
Nb_2O_5	n.a.	n.a.	n.a.	n.a.	0.13	n.a.	n.a.	—	n.a.	<0.01
NiO	n.a.	n.a.	n.a.	<0.01	n.a.	0.04	6.99	—	n.a.	0.02
Co	n.a.	n.a.	n.a.	n.a.	n.a.	<0.01	0.37	—	n.a.	<0.01
S	n.a.	n.a.	n.a.	n.a.	n.a.	38.52	<0.01	—	<0.01	0.09
F	n.a.	n.a.	n.a.	n.a.	n.a.	n.a.	n.a.	2.31	n.a.	0.02
Total	99.94	100.39	100.13	100.40	99.35	101.85	99.96	100.00	99.22	100.22
	An 86.1	Wo 3.3	Wo 33.5	Fo 70.6						
	Ab 13.2	En 69.4	En 45.2	Fa 29.4						
	Or 0.7	Fs 23.1								
	Others	4.2	8.1							
				Average—boulder # 2–5 samples						
Vol.%	59.9	22.9	5.8	7.7	1.6	0.1	0.1	0.8	0.9	
Wt.%	54.1	25.8	6.4	9.0	2.5	0.1	0.4	0.9	0.8	

*Elemental abundances; converted to oxides for calculating bulk composition.
†Assumed 1:1 mixture of fluorapatite and whitlockite.
n.a. = Not analyzed.

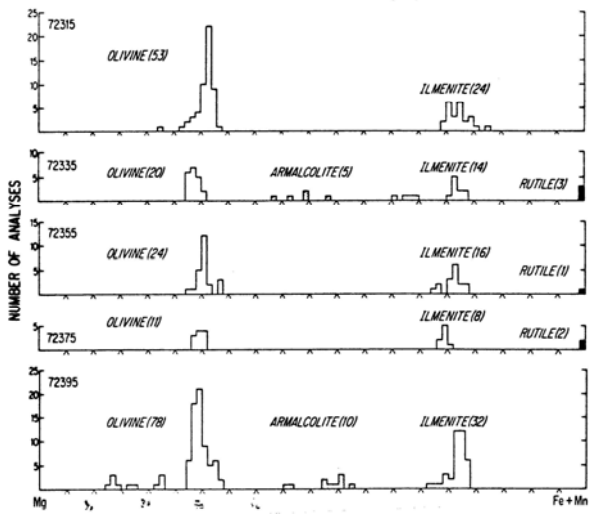

Figure 7: Compositions of olivines and Fe-Ti oxides in 72315, 72335, 72355, 72375, and 72395 (Dymek et al., 1976a).

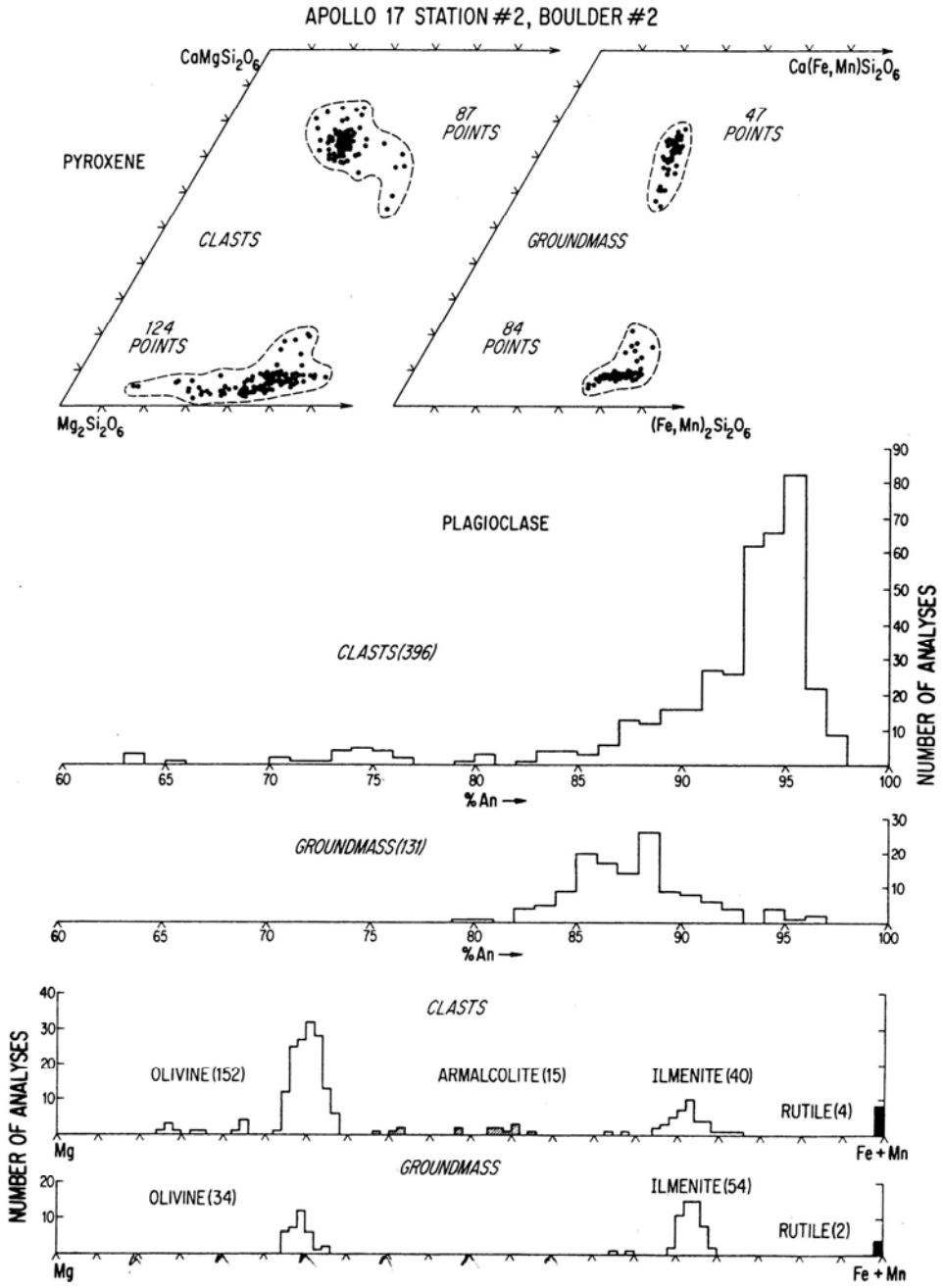

Figure 8: Summary diagram of mineral phases in 72315, 72335, 72355, 72375, and 72395 (Dymek et al., 1976a), distinguishing groundmass phases from clasts.

RADIOGENIC ISOTOPES

Tera *et al*. (1974a) reported U, Th, and Pb isotopic data for a whole-rock split of 72395 (Table 3) without specific discussion. As for other KREEP rocks, g (=$^{238}U/^{204}Pb$) is high, about 2200. The data lie on the same -3.9 - 4.4 Ga concordia curve as most highlands samples, and towards the lower age end as typical of brecciated KREEP rocks (model ages are in the range 4.06 to 4.09 Ga).

EXPOSURE AGES

Hutcheon et al. (1974b) and MacDougall et al. (1974) studied tracks in a column cut from 72395. Unfortunately the column was oriented parallel to the surface at 3 cm depth, so no depth variations could be measured. No systematic variations in track density occurred along the column. Track densities among adjacent feldspars vary between 2 and 5 x 10^6 cm-^{2}, far beyond statistical variation. The authors infer that shock erased some tracks about 11 Ma ago. Assuming a single stage irradiation, the maximum track density implies exposure of 27 Ma (from start of track accumulation at 3 cm depth. Fission tracks in an apatite crystal (Table 4) give ages of about 800 Ma, much younger than the probable crystallization age of the sample, suggesting a severe beating, or shock event exceeding 100 kb pressure.

PHYSICAL PROPERTIES

Charette and Adams (1977) measured the spectral reflectivity (0.5 to 2.5 microns wavelength range) of an interior chip of 72395, which they referred to as an "ANT-suite norite". The spectrum shows deep Fe^{2+} bands for pyroxene and plagioclase, with a high left shoulder near 0.7 microns. However, there is no absorption band near at 0.6 microns that would be indicative of ilmenite.

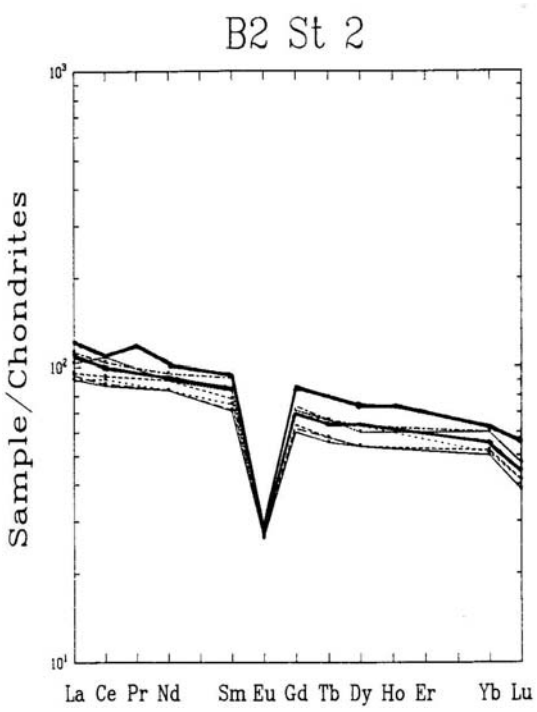

Figure 9: Rare earth elements in splits of 72395 (bold lines) and other Boulder 2, Station 2 samples. 72395 data from Table 2; upper bold line is 72395, 46; lower bold line is 72395,3.

Horai and Winkler (1976) measured the thermal diffusivity of a split of 72395 under varied conditions. The sample had a bulk density of 2.539 g/cm^3 and an intrinsic density of 3.073 g.cm^3. The porosity was 17.4 %. The diffusivity measurements are tabulated in Tables 5 and 6, and diagrammed in Figure 10.

PROCESSING

Following chipping of a few small pieces for petrographic and chemical study, 72395 was sawn into two pieces: ,7 and ,8 (Fig. 2). Between them slab pieces ,9 (29.5g),10 (25.2 g), and smaller pieces ,11 to ,26 were cut. Pieces were then chipped from,8 (now 59.8 g), as shown in Fig. 3. Many allocations were made from both the slab pieces and the fragments from ,8. ,7 is now 251.9 g, and ,8 (stored at WSTF) is now 59.8g.

Table 2: Chemical analyses of bulk samples of 72395.

Split	,3	,3	,46	,42	,43	,43	,3
wt %							
SiO_2			46.9				
TiO_2	1.7		1.75				
Al_2O_3	18.7		18.1				
Cr_2O_3	.210		0.2044				
FeO	9.2		9.29				
MnO	.116		0.12				
MgO	12		11.97				
CaO	11.0		11.27				
Na_2O	.67		0.694				
K_2O	.32		(c) 0.286				
P_2O_5			0.325				
ppm							
Sc	17		18.7				
V	50						
Co	35	33	31.1				
Ni	320	290	260				
Rb		5.3	6.21				
Sr		152	167				
Y							
Zr	400		570				
Nb							
Hf	12		13.7				
Ba	350	(a) 360	386				
Th	5.5		6.05				5.88
U	1.6	1.72	2.06		0.59	1.3	1.67
Cs		0.160	0.190				
Ta	1.6		1.82				
Pb							
La	36		39.7				
Ce	87		95				
Pr			13.1				
Nd	55		61				
Sm	15.2		16.8				
Eu	1.81		1.93				
Gd			21.1				
Tb	3.0		3.7				
Dy	20		23.2				
Ho			5.1				
Er			13.9				
Tm							
Yb	11		12.4				
Lu	1.5		1.88				
Li			24.8				
Be							
B							
C				105			
N							
S			560	770			
F			36		41		
Cl			9.90		(d) 8.4		
Br			.044		(d) 0.056		
Cu			3.55				
Zn		2.1	2.76				
ppb							
Au	5	5.8	4.7				
Ir	10	8.0	11				
I					(e) 1.7		
At							
Ga			4350				
Ge			440				
As			78				
Se		190					
Mo							
Tc							
Ru						17	
Rh							
Pd							
Ag		1.4					
Cd		(b) 170					
In		0.2					
Sn							
Sb		2.1					
Te							
W			750				
Re		0.79	0.2				
Os						9	
Pt							
Hg		0.29				4.4	
Tl							
Bi							
	(1)	(1)	(2)	(3)	(4)	(4)	(5)

References and methods:
(1) Laul and Schmitt (1974); INAA, RNAA
(2) Wanke et al. (1975a,b); XRF, INAA,RNAA
(3) Moore et al. (1974a,b); Cripe and Moore (1975)
(4) Jovanovic and Reed (1974a); RNAA
(5) Tera et al. (1974a);ID/MS

Notes:
a) listed by authors as Bd
b) contamination?
c) value of 0.2916 also tabulated
d) residue and leach combined
e) detected in leach only.

Table 3: U, Th, Pb isotopic data for 72395,3 (Tera et al, 1974).

Sample[a]	Weight mg	Lunar Lead[b,c] ^{208}Pb	^{207}Pb	^{206}Pb	^{204}Pb	α^d comp	conc	$^{204}Pb^b$ blank	$\Delta(^{204}Pb)^b$ blank	$^{204}Pb^e$ picomole/g
72395,3	9.628	55.58	26.63	59.11	0.0309	1294	1204	0.0185	0.0018	3.20 +0.97

[a] Total rock unless otherwise indicated. Acid washed samples designated by L; material removed from sample by acid wash designated by Leach. [b] In picomoles. [c] Corrected for blank with $\alpha = 18.26$, $\beta = 15.46$ and $\gamma = 37.59$. [d] Uncorrected for blank, α values for concentration runs (conc) are corrected for cross contamination from spikes. [e] Magnitude of negative error, corresponding to +100% increase in the blank, is twice the value given for the positive error shown, which corresponds to −50% decrease in the blank.

Sample[a]	^{238}U nanomole/g	^{232}Th nanomole/g	$\frac{Th}{U}^b$	$\frac{^{238}U^b}{^{204}Pb} \times 10^{-2}$	Model Ages (AE)[c,d] $\frac{207}{206}$	$\frac{206}{238}$	$\frac{207}{235}$	$\frac{208}{232}$
72395,3	6.96 ± 0.04	25.34 ± 0.25	3.61 ± 0.04	22 (+33, -5)	4.08	4.06	4.07	4.09

[a] Total rock analysis unless otherwise indicated. [b] Atomic ratios. [c] After correction for blank and primordial Pb. Assumed primordial compositions in $\alpha = 9.307$, $\beta = 10.294$ and $\gamma = 29.476$ (50).
[d] $\lambda_{238} = 1.5525 \times 10^{-10}\ y^{-1}$, $\lambda_{235} = 9.8485 \times 10^{-10}\ y^{-1}$ and $\lambda_{232} = 4.9475 \times 10^{-11}\ y^{-1}$.

Figure 10a: Thermal diffusivity (**K**) of 72395,14 as a function of temperature T with interstitial gas pressure 1 aim and 10-^{6} torr of air. Horai and Winkler (1976).

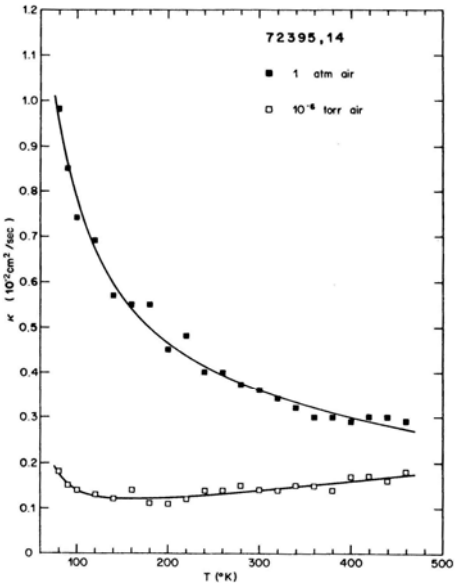

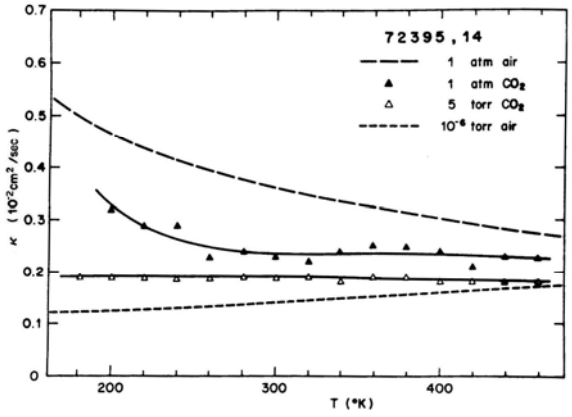

Figure 10b: Thermal diffusivity **(K)** of 72395,14 as a function of temperature T with interstitial gaseous pressure I atm and 5 torr of carbon dioxide. Smoothed curves of **K** as a function of T with interstitial gas pressure 1 aim and 10-^{6} torr are from Figure 10m Horai and Winkler (1976).

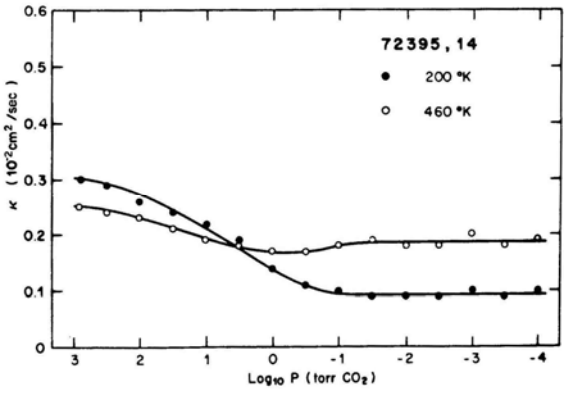

Figure 10c: Thermal diffusivity **(K)** of sample 72395,14 as a function of interstitial gas pressure P of carbon dioxide at temperatures of 200 degrees and 460 degrees K Horai and Winkler (1976).

Table 4: Fission track data for an apatite crystal in 72395 (Hutcheon S131,1974b).

	72395 Apatite
Uranium content (ppm)	108
Total track density (t/cm^2)	8.28×10^7
Reactor induced (t/cm^2)	4.22×10^7
Cosmic ray (t/cm^2)	3.0×10^6
C.R. induced fission* (t/cm^2)	4.22×10^7
Age† (m.y.) (a)	0
(b)	8.1×10^8

Table 5: Thermal diffusivity (K) (cm^2/sec) as a function of temperature T (degrees K), $I^j = A + B/r + C/1'^2 + DT^2$. Horal and Winkler (1976).

Sample	Condition	*A* (10^{-2} cm^2/sec)	*B* (cm^2 °K/sec)	*C* (10^2 cm^2 °K^2/sec)	*D* (10^{-8} cm^2/sec °K^2)
72395,14	1-atm air	0.207	0.488	0.090	−0.203
	10^{-6}-torr air	0.160	−0.154	0.133	0.190
	1-atm CO_2	0.816	−2.735	3.638	−0.789
	5-torr CO_2	0.214	−0.053	0.028	−0.121

Table 6: Thermal diffusivity (in the unit of 10'3 cm2/sec) of lunar solid rock samples under atmospheric conditions
(a) and under vacuum
(b). Horai and Winkler (1976).

	Temperature, degrees K.							
	100	150	200	250	300	350	400	450
a)	7.82	5.67	4.65	4.04	3.61	3.29	3.02	2.79
(b)	1.41	1.21	1.24	1.32	1.41	1.50	1.60	1.71